International Journal of Innovative Computing, Information and Control
Volume **9**, Number **5**, May **2013**

ICIC International ©2013 ISSN 1349-4198
pp. 2203–2228

DYNAMIC EVENTS ANALYSIS OF THAILAND AND MALAYSIA POWER SYSTEMS BY DISCRETE WAVELET DECOMPOSITION AND SHORT TERM FOURIER TRANSFORM BASED ON GPS SYNCHRONIZED PHASOR DATA

Issarachai Ngamroo

School of Electrical Engineering
Faculty of Engineering
King Mongkut's Institute of Technology Ladkrabang
Chalongkrung Rd., Ladkrabang, Bangkok 10520, Thailand
knissara@kmitl.ac.th

Received February 2012; revised June 2012

Abstract. *This paper applies the discrete wavelet decomposition and short term Fourier transformation to analyze the dynamic events in Thailand and Malaysia power networks using a synchronized phasor data obtained from the wide area monitoring system. The phasor data which are synchronized by global positioning system are measured from the 220 V wall outlets. Here, the dynamic analysis of two events is carried out. For the first event, a sudden 80 MW load transferring from Thailand to Malaysia systems through a weak 115 kV tie-line is considered. Second, the tripping of High-Voltage Direct Current link between Thailand and Malaysia due to the fault in a thyristor room at the converter station of Thailand side is analyzed. Both events cause a problem of frequency oscillation in a southern area of Thailand. Besides, they severely excite the inter-area oscillation in a 230 kV tie-line between central and southern areas of Thailand. Analyzed results based on discrete wavelet decomposition and short term Fourier transform provide valuable information of the system dynamic behavior in both frequency and time domains.*
Keywords: Discrete wavelet decomposition, Short term Fourier transform, Power system monitoring, Power system oscillations, Phasor measurement unit, Least-squares regression

1. **Introduction.** The interconnection between central and southern areas by 230 kV tie-line in Thailand 50 Hz electric power system establishes a longitudinal structure. This configuration causes the problem of inter-area oscillations [1,2]. Especially, the dominant inter-area oscillations with poor damping can deteriorate the dynamic stability of the system [3]. However, such inter-area oscillations between both areas have never been observed and analyzed before. The practical monitoring system as a smart power and energy management system is highly expected.

Recently, the phasor measurement units (PMUs) which are synchronized based on the time stamp of the global positioning system (GPS) [4,5] have been applied to power systems such as monitoring of power system dynamics [6,7], analysis of power system events [8,9], detection of transient power swing [10]. In these works, synchronized phasor measurement systems have been established at a high-voltage transmission level. To increase the feasibility of the wide area monitoring of power system oscillations, a new monitoring system with convenient installation at a distribution level, high accuracy of the measured data, Internet based data transmission, and cost-effective is highly expected. To achieve these requirements, the Internet based GPS synchronized wide area frequency monitoring network (FNET) developed at the 110-V distribution level has been established in US

system [11]. The objective of FNET is to create an extremely low cost and quickly deployable wide area frequency measurement system. Moreover, the power system frequency can be accurately measured and synchronized at 110-V typical demand side outlet. Many applications of FNET are described in [11].

In this paper, a wide area dynamic stability monitoring system in Thailand power network is developed. The monitoring system is established by GPS-synchronized PMUs. The salient feature of the monitoring system is the convenient installation of PMUs at 220 V domestic outlets. Besides, the initial installation cost is very low. In the proposed system, PMUs are located at two universities which represent central and southern areas of Thailand power system. The PMU data transmission between both universities is performed via the Internet. The phase difference between two universities can be calculated from phasor voltages collected by PMUs. By using the phase difference data, the physical characteristics of power oscillations can be analyzed.

Here, the discrete wavelet decomposition and short term wavelet transform are applied to analyze two dynamic events of Thailand and Malaysia power systems. For the first event, an 80 MW load transferring from Thailand to Malaysia systems through a weak 115 kV tie-line is considered. To perform load transferring, a synchronization between both systems is required. For the second event, the tripping of High-Voltage Direct Current (HVDC) link between Thailand and Malaysia due to the fault in a thyristor room at Khlong Ngae converter station of Thailand side. Both events cause a problem of frequency oscillation in a southern area of Thailand, which is analyzed. Besides, they severely activate the inter-area oscillation in a 230 kV tie-line between central and southern areas of Thailand. Analyzed results give clear physical understanding of the system dynamic behavior in both frequency and time domains.

The organization of this paper is as follows. First, the proposed monitoring system is described in Section 2. Next, the overview of interconnection between Thailand and Malaysia power systems is explained in Section 3. Section 4 presents the analysis method. Subsequently, the analysis of 1st and 2nd power system events are carried out in Sections 5 and 6, respectively. Section 7 talks about identification of power oscillation mode. Lastly, a conclusion is given.

2. **Proposed Monitoring System.** An overview of the Thailand power system is delineated in Figure 1. The Electricity Generation Authority of Thailand (EGAT) is responsible for generation and transmission grids of high voltage levels. Central and southern areas are connected by 230 kV tie-line with 800 km long. This interconnection establishes a longitudinal structure between both areas which may cause an inter-area oscillation. To monitor the inter-area mode between both areas, PMUs are located at King Mongkut's Institute of Technology Ladkrabang (KMITL), Bangkok and Prince of Songkla University (PSU), Songkla, which represent central and southern areas, respectively.

Figure 2 shows the proposed PMU-based monitoring system via conventional power outlets. The phasor measurement system employs a manufactured PMU as a commercial product, which is a Network Computing Terminal Type-A, NCT2000 of Toshiba [12,13]. The PMU can measure a single-phase instantaneous voltage at 220 V outlet, with correcting its clock based on the time stamps of GPS. As the PMU uses the time stamps of GPS for its clock correction, the time synchronization between PMUs located at distant places is easily accomplished by keeping their internal clocks synchronous with the time stamps of GPS. As given in [13,14], the phasor voltage is computed by

$$\overset{\bullet}{V} = \frac{\sqrt{2}}{N}\left\{\sum_{k=1}^{N} V_k \sin k\theta + j\sum_{k=1}^{N} V_k \cos k\theta\right\} \tag{1}$$

where $\dot{V}$ is the phasor voltage, V_k is a sequential data of the instantaneous voltage of 220 V outlet sampled by an A/D converter, N is the sampling number of the voltage and θ is the sampling angle. For this apparatus, $N = 96$ and $\theta = 2\pi/N$ 3.75deg.

Based on (1), the phase angle can be calculated by

$$\delta = \tan^{-1}\left[\mathrm{Im}\left(\dot{V}\right)\Big/\mathrm{Re}\left(\dot{V}\right)\right] \tag{2}$$

where $\mathrm{Re}(\dot{V})$ and $\mathrm{Im}(\dot{V})$ are the real part and the imaginary part of the phasor voltage $\dot{V}$, respectively. The phase angle δ is accumulated in the PMU as the time sequential data. Calculation in (2) provides phase angle referred to the GPS time. The PMU records the calculated phasor voltages every 40 ms (2 cycles) and measures at the domestic outlets for 20 minutes twice an hour, for example, 0.20-0.40 a.m. and 0.50-1.10 a.m. Hence, there are 30,000 data of phasor voltages for 20 minutes. The measured phasor voltages at PSU are transmitted via the Internet to a server at KMITL.

The significance of the proposed system can be clearly explained relative to previous works as follows.

In the previous works, synchronized phasor measurement systems have been established in a power transmission level. The synchronized phasor measurement have been successfully installed transmission level in China [14], Eastern Denmark [15] and United State [16], etc. Nevertheless, these installation costs of these systems are very high. In addition, since these monitoring systems belong to the power companies, it is difficult for researchers to access the measured data.

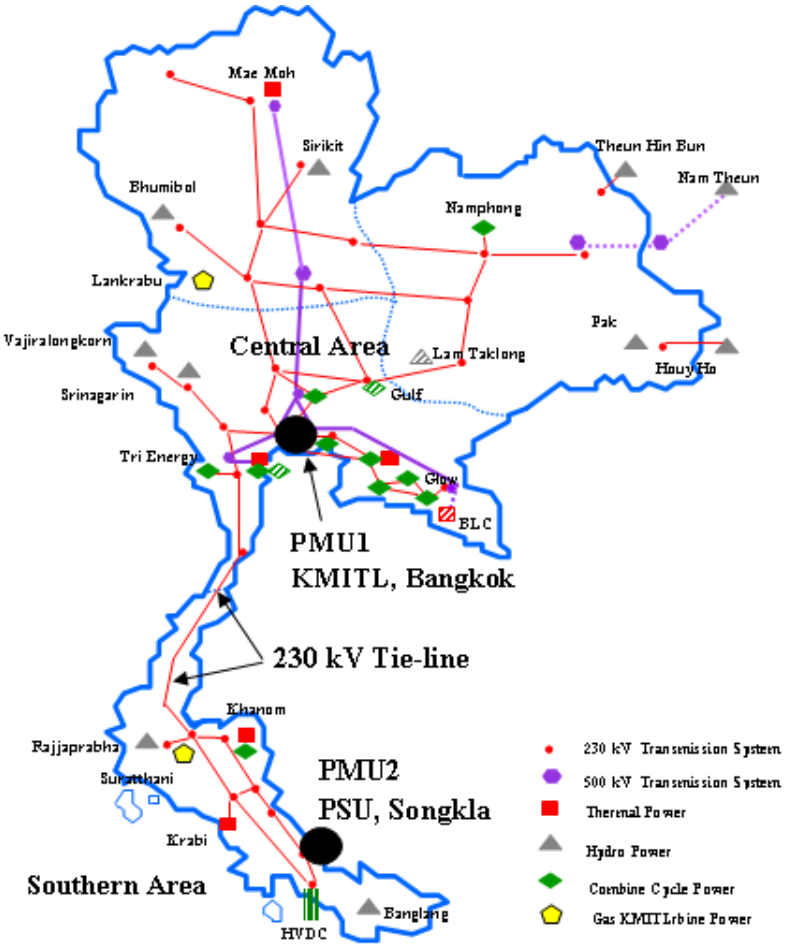

FIGURE 1. Location of PMUs

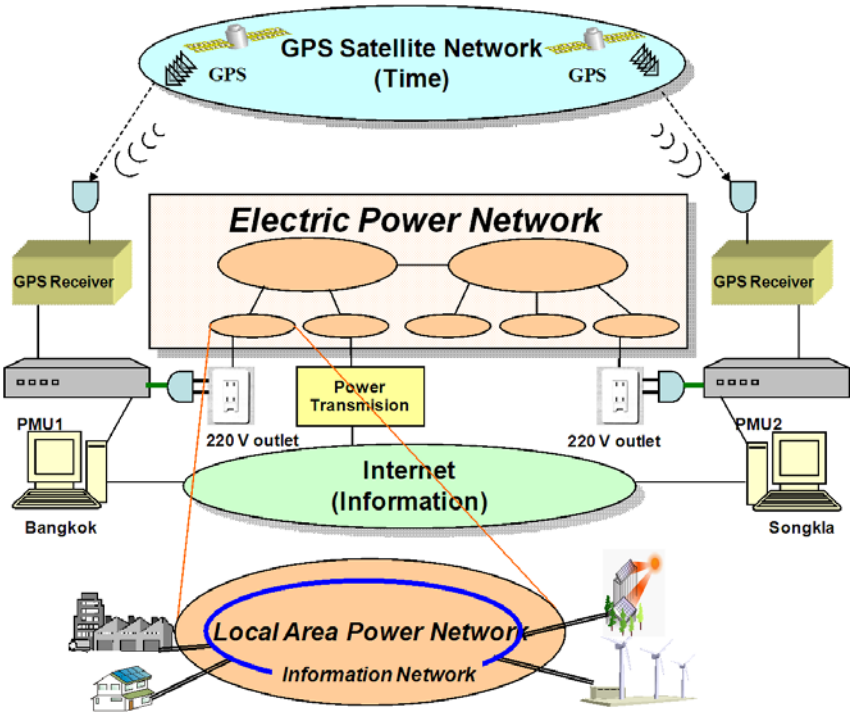

FIGURE 2. Proposed PMU based monitoring system via 220 V outlet

To increase the feasibility of the wide area monitoring of power system oscillations, a new monitoring system with convenient installation at a distribution level, easy access for researchers, high accuracy of the measured data, Internet based data transmission, and cost-effective is highly expected. To cope with all significances aforementioned, the paper proposes the wide area monitoring of power system oscillations based on the GPS-synchronized PMUs via 220 V demand side outlets. The proposed system not only requires very low capital cost, but also provides high accuracy of the measured data. Besides, it is very useful for researchers, university students to access the data. Furthermore, the proposed system is the first wide area monitoring system based on wall outlet in Thailand. The proposed system can be applied to on line system analysis such as an intelligent voltage control system [17] and a fault detection in power systems [18-20].

3. Overview of Interconnection between Thailand and Malaysia Power Systems.

As shown in Figure 3, there are two interconnections between Thailand and Malaysia power systems, i.e., a 115 kV AC link and an HVDC link. The EGAT can exchange electricity with the Tenaga Nasional Berhad (TNB) through AC and DC interconnections.

4. Analysis Method.

4.1. Discrete wavelet decomposition.

The wavelet decomposition (transform) [21] is a mathematical tool, much like a Fourier transform in analyzing a stationary signal. The basis functions used in Fourier analysis are precisely located in frequency but exist for all time. The frequency information of a signal calculated by the classical Fourier transform is an average over the entire time duration of the signal. Thus, if there is a local transient over some small interval of time in the lifetime of the signal, the transient will contribute to the Fourier transform but its location on the time axis will be lost. Although the short-time Fourier transform overcomes the time location problem to a large extent, it does not

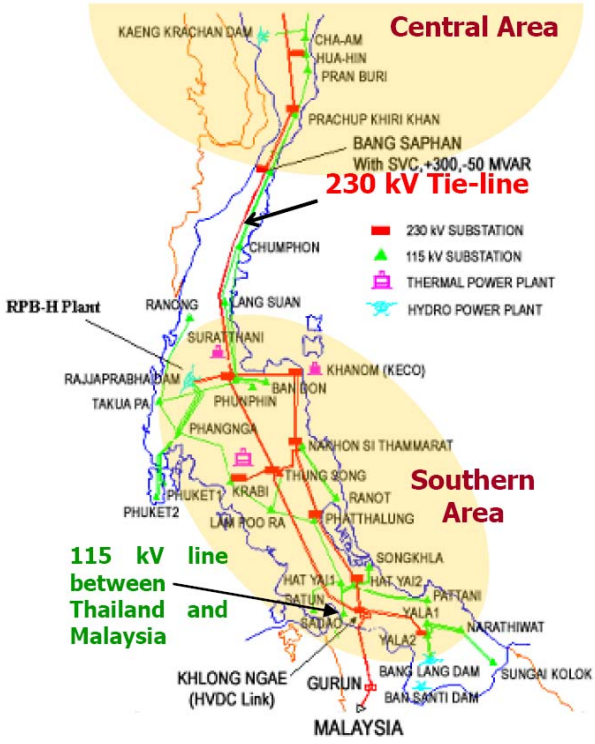

FIGURE 3. Tie-line interconnection between Thailand and Malaysia

provide multiple resolution in time and frequency, which is an important characteristic for analyzing transient signals containing both high and low frequency components.

Wavelet analysis overcomes the limitation of Fourier methods by employing analyzing functions that are local both in time and frequency. These wavelet functions are generated in form of translations and dilations of a fixed function, this called mother wavelet. The wavelet decomposes a signal into different scales with different levels of resolution by dilating a single prototype function. The decomposition into scales is made possible by the fact that the wavelet transform is based on a square-integrable function and group theory representation. Furthermore, unlike the Fourier transform which gives a global representation of a signal, the wavelet transform, on the other hand, provides a local representation (in both time and frequency) of a given signal; therefore, it is suitable for analyzing a signal where time-frequency resolution is needed.

The discrete wavelet decomposition has been applied to many researchers such as an abnormal signal extraction [22], an image encryption algorithm [23], a robust reversible data hiding scheme [24], a design and analysis of network traffic methods [25], an identification of fault location for simultaneous fault in distribution system [26], a hemodynamic analyzing method for FMRI data [27], an image fusion [28], a classification of Stego and PS images [29], a Chinese minority script identification [30], a classification of sound types in border monitoring system [31], a pitch detection [32].

The mathematical definitions are explained as follows. Let $x(t)$ be a signal defined in $L^2(\Re)$ space, which denotes a vector space for finite energy signals. $\Re$ is a real continuous number system. Such signals satisfy

$$\int_{-\infty}^{\infty} |x(t)|^2 \, dt < \infty \tag{3}$$

The continuous wavelet transform (CWT) of $x(t)$ is defined as

$$CWT_\psi x(a,b) = W_x(a,b) = \int_{-\infty}^{\infty} x(t)\psi^*_{a,b}dt \tag{4}$$

where

$$\psi_{a,b}(t) = |a|^{-1/2}\,\psi\left(\frac{t-b}{a}\right) \tag{5}$$

$\Psi(t)$ is the base function or the mother wavelet, the asterisk denotes a complex conjugate, and $a, b \in \Re$, $a \neq 0$, are the dilation and translation parameters, respectively.

Since the transformation is achieved by dilating and translating the mother wavelet continuously over $\Re$, it generates substantial redundant information. Therefore, instead of continuous dilation and translation, the mother wavelet maybe dilated and translated discretely by selecting $a = a_0^m$ and $b = nb_0a_0^m$, where a_0 and b_0 are fixed constants with $a_0 > 1$, $b_0 > 0$, $m, n \in$ Z, and Z is the set of positive integers. Then, the discretized mother wavelet becomes

$$\psi_{m,n}(t) = a_0^{-m/2}\psi\left(\frac{t - nb_0a_0^m}{a_0^m}\right) \tag{6}$$

and the corresponding discrete wavelet transform is given by

$$DWT_\psi x(m,n) = \int_{-\infty}^{\infty} x(t)\psi^*_{m,n}dt \tag{7}$$

where $\psi_{m,n}(t)$ is given in (6). In this work, the Symlet wavelets function is selected as the mother wavelet.

4.2. **Short-term Fourier transform.** One of the shortcomings of the Fourier transform is that it does not give any information on the time at which a frequency component occurs. One approach which can give information on the time resolution of the spectrum is Short-term Fourier transform (STFT) [33]. The STFT is a signal processing method used for analyzing non-stationary signals, whose statistic characteristics vary with time. In essence, STFT extracts several frames of the signal to be analyzed with a window that moves with time. If the time window is sufficiently narrow, each frame extracted can be viewed as stationary so that Fourier transform can be used. With the window moving along the time axis, the relation between the variance of frequency and time can be identified.

The STFT has been applied to a three-dimensional profile acquisition method [34] and a vibration signal recognition [35], etc.

Given the time-series $x[n]$, the STFT at time n is given as

$$X(n,\omega) = \sum_{m=-\infty}^{\infty} x\,[m]\,w\,[n-m]e^{-j\omega m} \tag{8}$$

where $w[n]$ is the analysis window, which is assumed to be non-zero only in the interval $[0, N_w - 1]$. The STFT can be also written as

$$X(n,\omega) = \frac{1}{2\pi}\int_{-\pi}^{\pi} W\,(\theta)e^{-j\theta n}X\,(\omega+\theta)\,d\theta \tag{9}$$

$X(\omega)$ is the Fourier transform of $x[m]$ and $W(-\omega)e^{j\omega n}$ as the Fourier transform of $w[n-m]$ with respect to m. The size of $w[n]$ affects the time-frequency resolution of STFT as shown

in Table 1. A fundamental problem of STFT and other time-frequency analysis technique is the selection of the windows to achieve a good trade-off between time and frequency resolutions.

Since the phasor data is the random signal, the Hanning window which is best for the random signal, is selected so that both time and frequency resolutions can be achieved.

The set-up of the parameters in the discrete wavelet decomposition based on the MATLAB Wavelet Toolbox [36] is given in Table 2.

The set-up of the parameters in the Short-time Fourier transform based on the MATLAB Signal Processing Toolbox [37] is given in Table 3.

5. **Analysis of 1st Power System Event.** The system event considering here is the transferring of partial loads about 80 MW at Sadao 115 kV substation in Thailand side to the Malaysia power grid. To transfer loads, a synchronization between both system is required. The phase difference data recorded by PMUs during synchronization are collected and used to analyze a system dynamic behaviour.

TABLE 1. Trade-off between time and frequency resolution

Window size of $w[n]$	Bandwidth of $W(\omega)$	Time resolution	Frequency resolution	Good For
long	narrow	bad	good	Sinusoidal components (harmonics)
short	wide	good	bad	Fast time-varying components

TABLE 2. Parameters setting for discrete wavelet decomposition

Maltab Command	Meanings and setting
WAVEDEC(X, N, 'wname')	performs a multilevel 1-D wavelet analysis using either a specific wavelet 'wname' or a specific set of wavelet decomposition filters
X	Input signal
N	Number of levels
wname	Specific wavelet "sym8"

TABLE 3. Parameters setting for short-time Fourier transform

Maltab Command	Meanings and setting
SPECTROGRAM (X, WINDOW, NOVERLAP, F, Fs)	Performs a short-time Fourier transform
X	Input signal
WINDOW	Hanning
NOVERLAP	The number of samples each segment of X overlaps = 30
F	FFT length = 1024
Fs	Number of sampling = 512

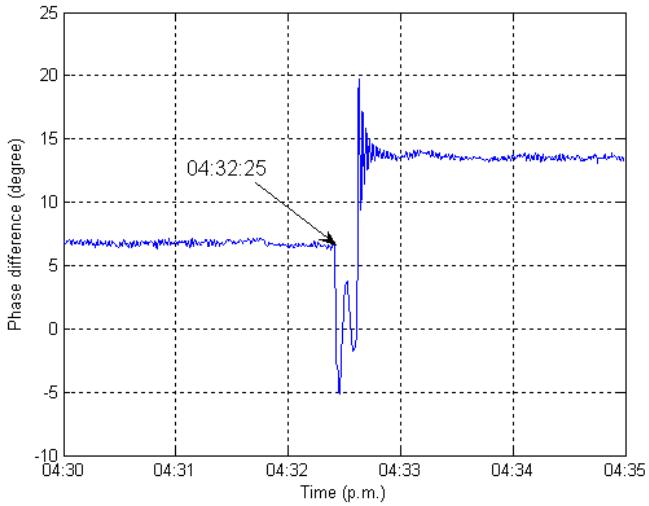

FIGURE 4. Phase difference between Bangkok and Songkla of PMUs

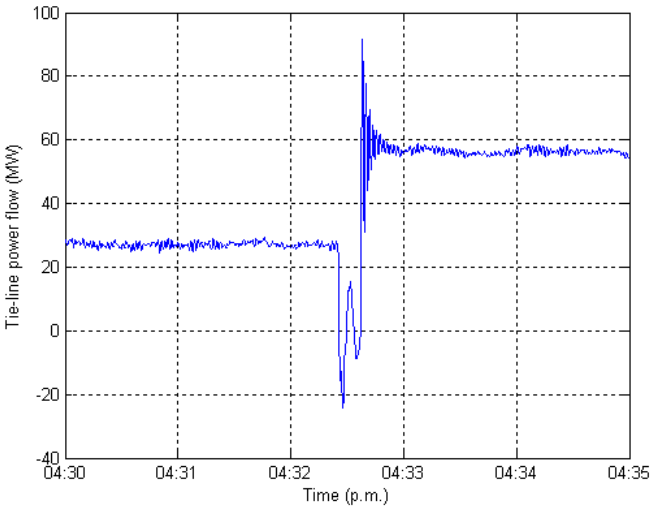

FIGURE 5. Active power flow of EGAT

Figure 4 depicts a waveform of phase difference between Bangkok and Songkla from 4.30 p.m. to 4.35 p.m. on March 20, 2006. The load transferring by synchronization of two systems has been performed at 04:32:25 p.m. In a phase difference signal, there are both positive and negative phase differences. The positive phase difference implies that the real power flows from the central area to the southern area and vice versa. Moreover, the phase difference between two interconnected areas reflects the active power flow in a 230 kV tie-line between both areas.

To verify the validity of the PMU data, the phase difference is compared with the actual power flow of a 230 kV tie-line between central and southern areas of EGAT as demonstrated in Figure 5. Obviously, the phase difference changes in the same fashion as the power flow.

Next, the correlation between the tie-line power flow data of EGAT and phase difference data measured by PMUs is evaluated by a least-squares regression [38]. The applications of least square regression has been applied to degree reduction of B-spline curves with

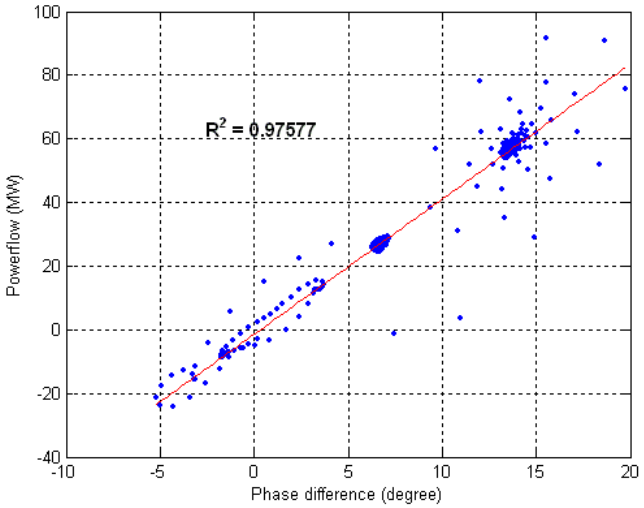

FIGURE 6. Least-squares linear equation

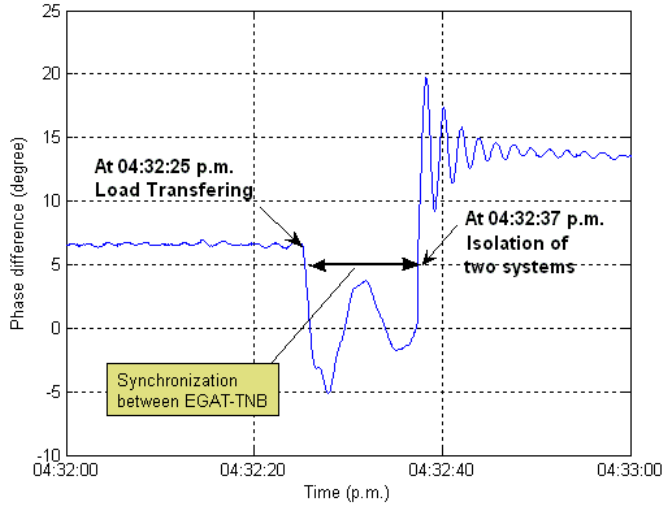

FIGURE 7. Amplified phase difference wavefrom between Bangkok and Songkla

multiple knots in [39]. The linear equation with two variables is used as a regression model. The resulted least-squares linear equation of the power flow and phase difference can be delineated in Figure 6.

To evaluate the fitness of both data, the correlation coefficient between two variables is calculated by

$$R^2 = \left[\frac{n\left(\sum xy\right) - \left(\sum x\right)\left(\sum y\right)}{\sqrt{\left[n\sum x^2 - \left(\sum x\right)^2\right]}\sqrt{\left[n\sum y^2 - \left(\sum y\right)^2\right]}} \right]^2 \tag{10}$$

where x is phase difference data, y is power flow data, and n is a number of data. The correlation coefficient R^2 indicates the fitness of data. If R^2 is close to unity, then the power flow strongly correlates with the phase difference. If not, the correlation is weak. As given in Figure 6, the correlation coefficient of two variables is nearly equal to one. The phase difference data measured by PMUs strongly correlates with the power flow

data of EGAT. This confirms the validity of the phase difference data of PMUs measured from 220 V wall outlets.

Figure 7 shows the amplified waveform of phase difference during load transferring. At 04:32:25 p.m. both systems are synchronized via a 115 kV line. Thailand system imports electricity from the Malaysia system to supply 80 MW loads. It can be seen that the phase difference between both areas abruptly changes and tends to severely oscillate during synchronization. After the load transferring is completed, both systems are isolated at 4:32:37 p.m. The phase difference immediately increases and oscillates. Eventually, the phase difference reaches a new steady-state value.

Next, the system frequency during load transferring is calculated from phase data at each PMU's location. The time derivative of phase angle corresponds to the deviation of system frequency. Accordingly, the frequency deviation is calculated by

$$\Delta f_n = \frac{\delta_{n+1} - \delta_n}{360 \Delta t_n} \tag{11}$$

where Δt_n is a sampling interval of sequential phase angle data δ_n at each location, that is 1/25 second and n is the number of accumulated phase angle data. Therefore, the variation of frequency at either location can be observed by PMUs with accumulating the sequential frequency deviation data Δf_n.

Figure 8 depicts the frequency deviations of Bangkok and Songkla during the event. Before load transferring, frequency deviations of both locations are almost the same. At 04:32:25 p.m. the frequency deviation of Songkla abruptly increases. It begins to oscillate and tends to apart from the frequency deviation of Bangkok. The central and southern areas cannot synchronize well. During load transferring, the southern area is connected to both central areas of Thailand and Malaysia systems. As a result, Thailand system swings against Malaysia system. This is equivalent to an oscillation between two machines through a weak tie-line. Stability of both systems may be deteriorated if a synchronous link is still performed. To prevent the electricity interruption, it is necessary to perform a synchronous link in a few seconds during load transferring. At 04:32:37 p.m., Thailand system is isolated from Malaysia system. The partial loads of EGAT transmission grid are completely transferred to the TNB, Malaysia. At the time of system isolation, the inter-area mode is also excited again, the oscillation is more dominant than that during

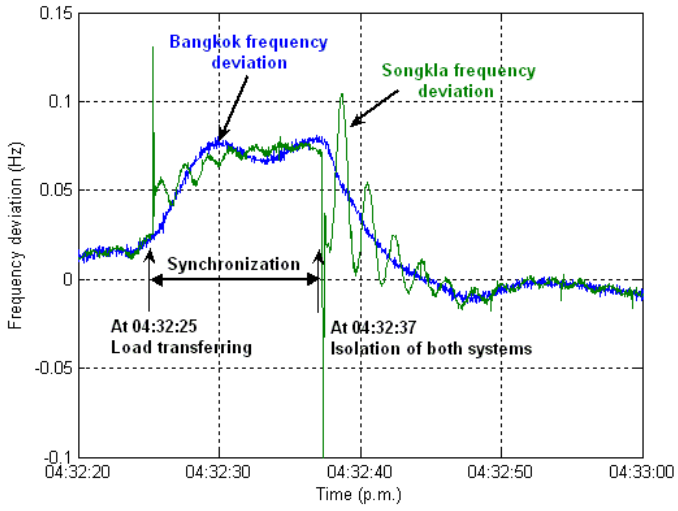

FIGURE 8. Frequency deviations of Bangkok and Songkla

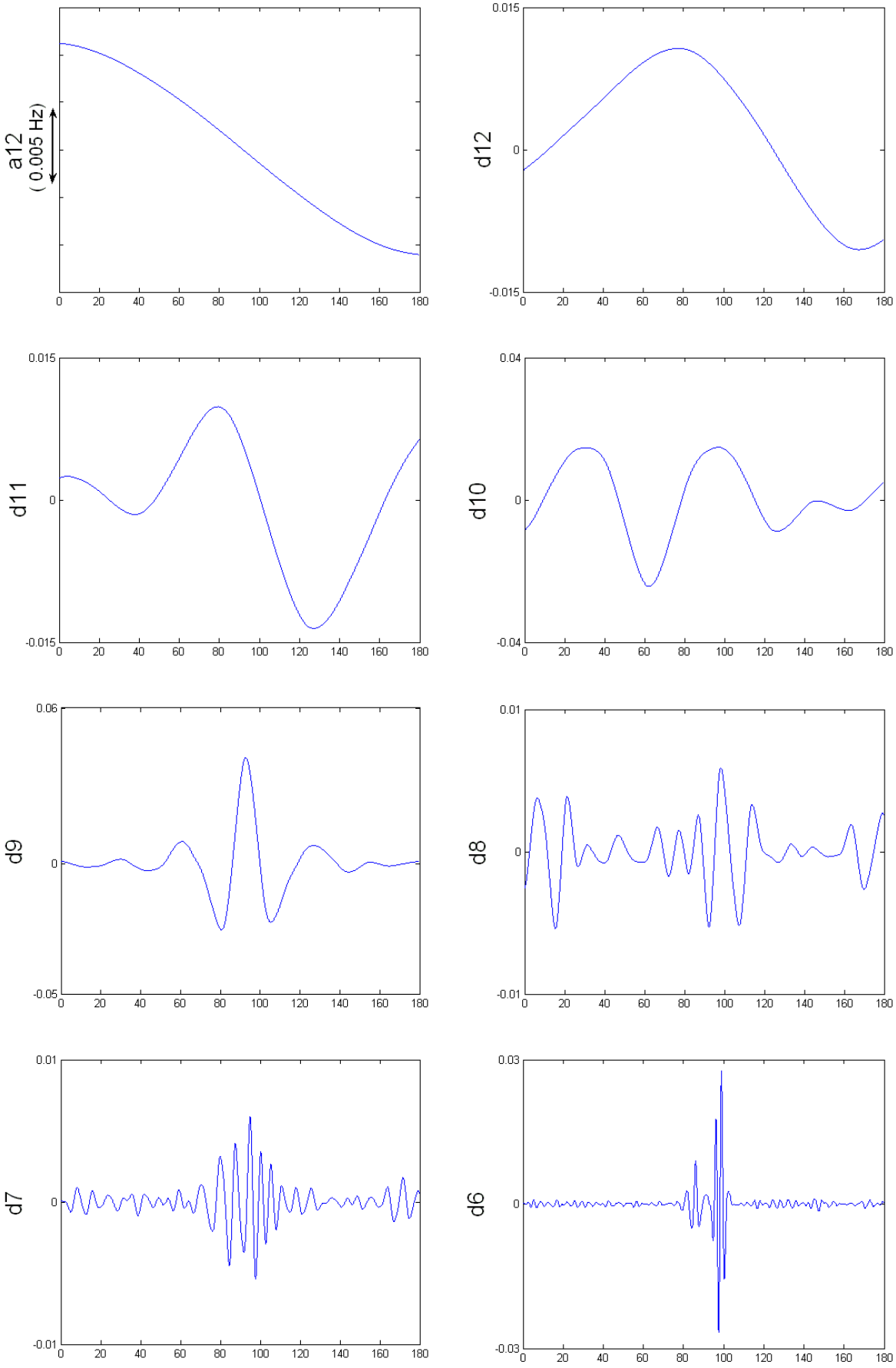
a12
(0.005 Hz)
d12
d11
d10
d9
d8
d7
d6

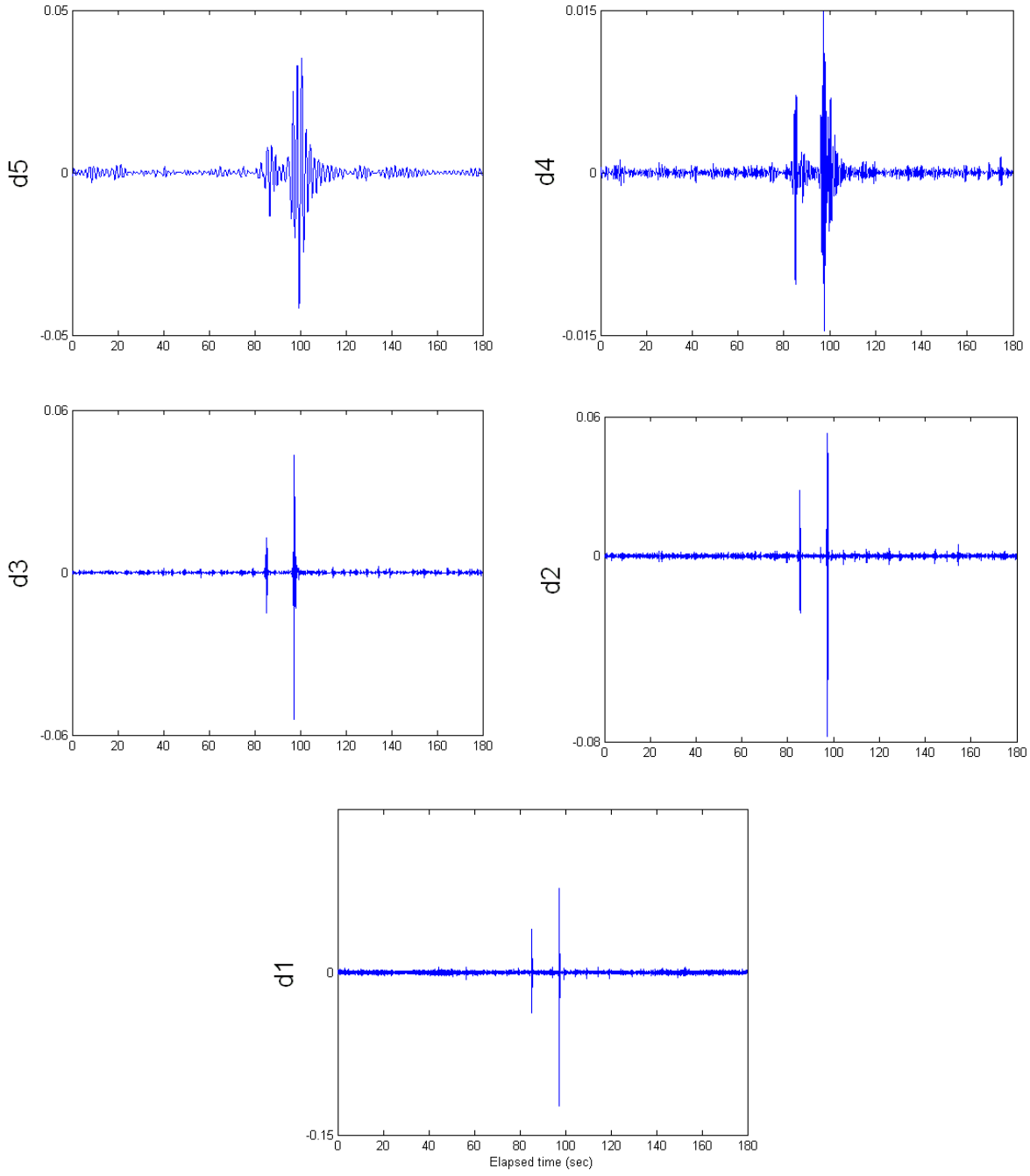

FIGURE 9. Wavelet decomposition results of Songkla frequency deviation

system synchronization. Subsequently, the frequency deviation of Songkla damps out and synchronizes with that of Bangkok again.

Next, the impact of load transferring on the inter-area oscillation mode in a 230 kV tie-line between central and southern areas of Thailand system is investigated. It can be observed in Figure 8 that the frequency deviation at Songkla oscillates at the frequency of the inter-area mode (0.2-0.8 Hz) [40]. To extract the signals with the frequency of the inter-area mode from the Songkla frequency deviation, the discrete wavelet decomposition is applied. Here, the Symlet wavelets function with 12 levels is used to decompose the frequency deviation signal of Songkla from 04:31 p.m. to 04:34 p.m. Figure 9 depicts the wavelet decomposition results which consist of 12 detailed components (d1-d12) and

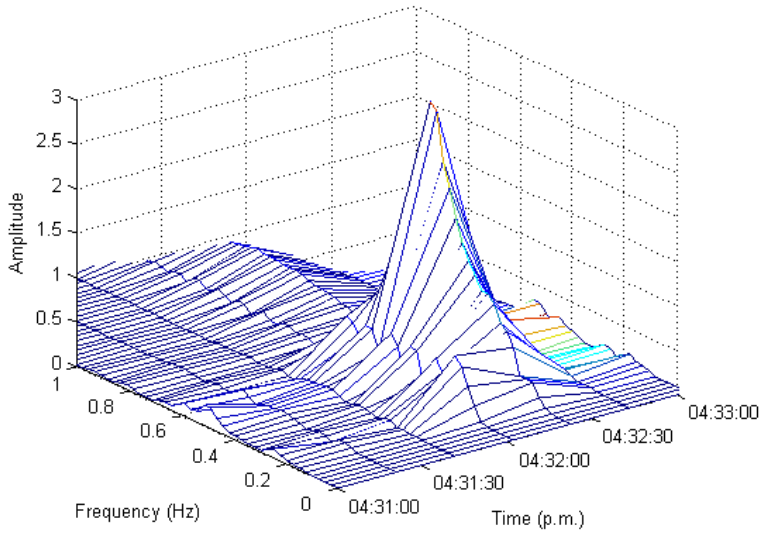

FIGURE 10. Frequency characteristic of the frequency deviation analyzed by short-time Fourier transform

the approximated component (a12). Based on analyzed results, the oscillation frequency of the dominant inter-area mode is around 0.4-0.6 Hz. To find the detailed components which have an oscillation frequency in the range of the dominant inter-area mode, the Fast Fourier Transform is applied. As a result, the frequency ranges of the wavelet d4, d5 and d6 elements are 0.6-2.0 Hz, 0.2-1.1 Hz and 0.17-0.6 Hz, respectively. Thus, d4, d5 and d6 elements are in the vicinity of the inter-area oscillation mode. The summation of d4, d5 and d6 signals (d4+d5+d6) are used to analyze the dynamic characteristic of the inter-area mode.

To demonstrate the characteristic of the inter-area mode in both frequency and time domains, the Short-time Fourier Transform is applied to the d4+d5+d6 signals. Figure 10 illustrates the frequency characteristic of frequency deviation analyzed by Short-time Fourier transform. It can be observed that the dominant inter-area mode about 0.4-0.6 Hz occurs at 04:32:25 p.m. same as appeared in the frequency deviation of Songkla. The short period of synchronization between Thailand and Malaysia systems via 115 kV line as well as the isolation of both systems significantly excite the inter-area oscillation mode in a 230 kV tie-line.

6. **Analysis of 2nd Power System Event.** The 300 MW Thailand – Malaysia HVDC interconnection system consists of Khlong Ngae converter station on the Thai border and Gurun converter station on the Malaysia border as shown in Figure 11. Both stations are linked by a 300 kV DC overhead transmission line with 110 km long. Khlong Ngae converter station operated by EGAT is situated at Sadao district in Southern Songkla province, about 24 km from Thai-Malaysia border. On the other hand, Gurun converter station governed by Tenaga Nasional Berhad (TNB), Malaysia power company, is located in Kedah, about 86 km from Malaysia's northern border.

The primary objective of the HVDC interconnection between both countries is the emergency assistance and economic power exchange due to the time difference in peak demand of the two systems. Besides, the HVDC system could provide solutions to the synchronization problem between two systems. It also allows full bi-directional control of

FIGURE 11. HVDC link between Thailand and Malaysia

TABLE 4. Time sequence of events

No.	Time	Event
1	2:30 a.m.	Tie-line power was –1.1 MW power flows from southern area to central area.
2	2:58:52 a.m.	HVDC was tripped due to fault in thyristor room at Klong Ngae Converter Station (Thailand Side) when received 300 MW from TNB, Malaysia.
3	3.00 a.m.	Tie-line power is increased to 272.4 MW and flows from central area to southern area.
4	6:30 a.m.	HVDC is operated again while tie-line power was 320.2 MW.
5	6.39 a.m.	HVDC received power 300 MW from TNB.
6	7:00 a.m.	Tie-line power is reduced to 25 MW.

power interchange and improves reliability and dynamic performance of both AC transmission systems.

The power system event considering here is the tripping of the HVDC link between Thailand and Malaysia due to the fault in the thyristor room at Klong Ngae station of Thailand side at 2:58:52 a.m. on July 22, 2005. The event occurred when the HVDC link of EGAT received 300 MW from TNB. The time sequence of events is given in Table 4.

Figure 12 shows the phase difference between Bangkok and Songkla recorded by PMUs. Prior to 2:58:52 a.m. the phase difference is about –9 deg. The negative phase difference means that the tie-line power flows from southern area to central area. This negative phase difference is consistent with the actual tie-line power flow of EGAT on July 22, 2005 as shown in Figure 13. The power flow at 2:30 a.m. is about –1.1 MW. Note that the power flow data of EGAT are measured at every half hour.

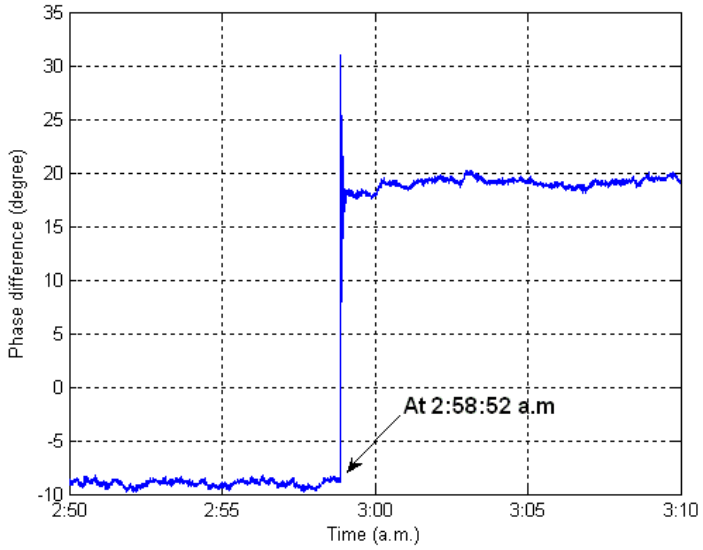

FIGURE 12. Phase difference between Bangkok and Songkla

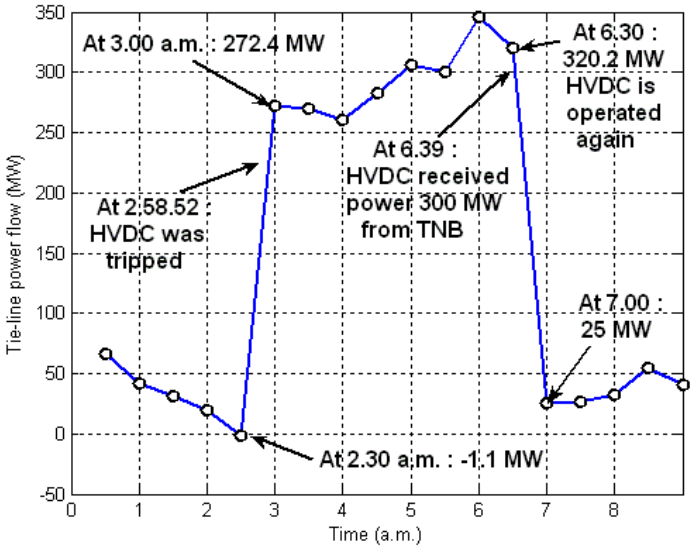

FIGURE 13. Actual tie-line power flow of EGAT

When the HVDC was tripped at 2:58:52 a.m., the phase difference abruptly increases to a very high positive value and settles down at about +19 deg. This implies that the direction of power flow is also suddenly changed. As depicted in Figure 13, the tie-line power flow from central area to southern area is 272.4 MW at 3:00 a.m. The support power from central area is used as an emergency assistance to serve loads in the southern area.

Next, the system frequency during the tripping event is considered. The time derivative of phase angle corresponds to the deviation of system frequency. Accordingly, the frequency deviation can be calculated by (4). Therefore, the variation of system frequency can be observed by the PMU with accumulating the sequential frequency deviation data Δf_n. Figure 14 shows frequency deviations of Bangkok and Songkla. At 2:58:52 a.m. the frequency deviation of Songkla instantaneously drops to –0.6 Hz. Subsequently, the

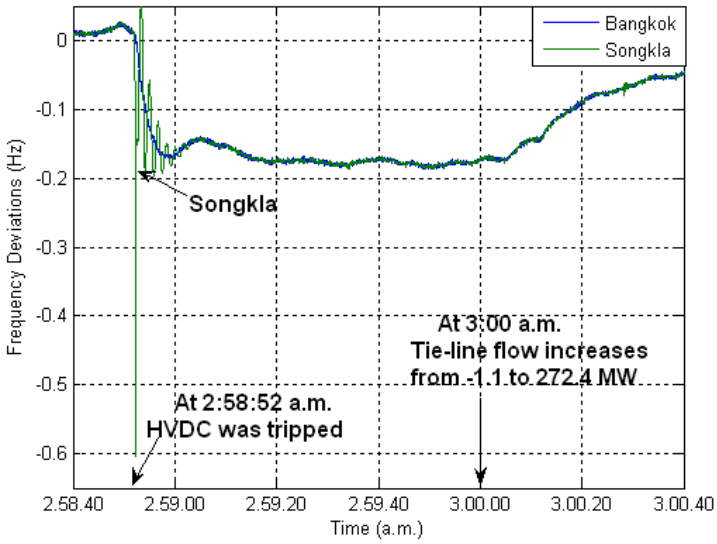

FIGURE 14. Frequency deviations of Bangkok and Songkla

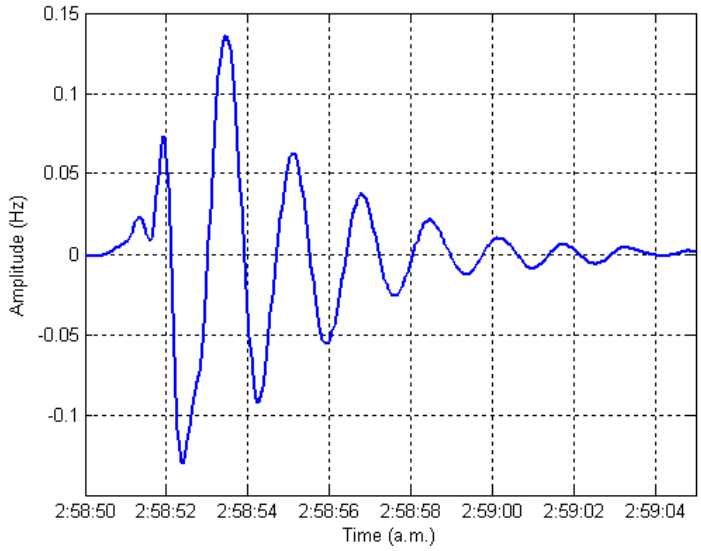

FIGURE 15. Wavelet d4+d5+d6 component at tripping time

inter-area oscillation appears in the frequency deviation of Songkla. This signifies that the tripping of HVDC link excites the inter-area mode to oscillate. After the oscillation subsides, the frequency deviations drops about –0.19 Hz for one minute until 3.00 a.m. Because the tie-line power flow supported from central area increases to 272.4 MW at 3:00 a.m. as in Figure 14, the frequency deviations start to recover.

To extract the dominant inter-area oscillation appeared in the frequency deviation of Songkla, the discrete wavelet decomposition is applied. Here, the Symlet wavelet with 12 levels is used to decompose the frequency deviation signal from 2:57 a.m. to 3:00 a.m. As a result, the frequency ranges of the wavelet d4, d5 and d6 elements are 0.6-2.0 Hz, 0.2-1.1 Hz and 0.17-0.6 Hz, respectively. Thus, d4, d5 and d6 elements are in the vicinity of the inter-area oscillation mode (0.2-0.8 Hz). Therefore, the summation of d4, d5 and

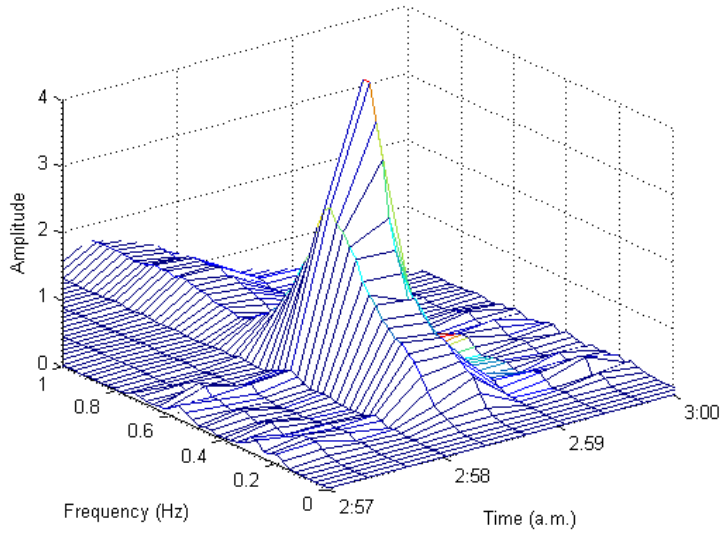

FIGURE 16. Frequency characteristic of frequency deviation analyzed by short time Fourier transform

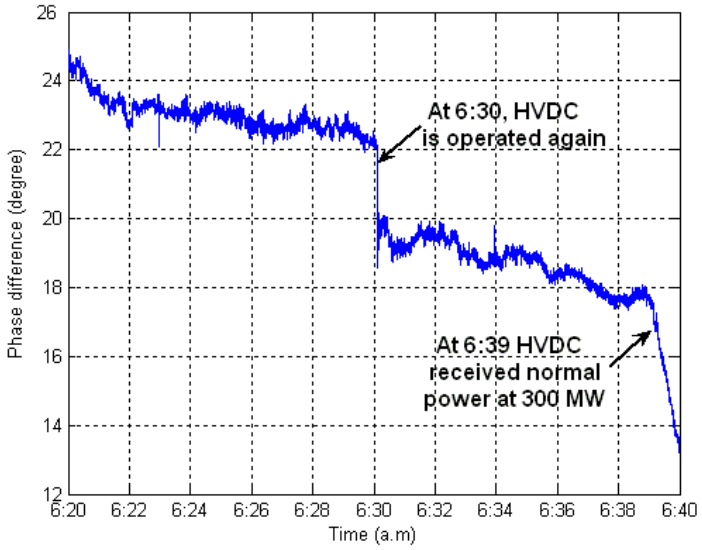

FIGURE 17. Phase difference between Bangkok and Songkla

d6 (d4+d5+d6) are used to analyze the dynamic characteristic of the inter-area mode. Figure 15 depicts the waveform of d4+d5+d6 at the tripping time.

Next, the short-time Fourier transform is applied to wavelet d4+d5+d6 elements. Figure 16 illustrates the frequency characteristic of frequency deviation analyzed by short time Fourier transform. It can be observed that the dominant inter-area mode about 0.5-0.6 Hz occurs at 2:58:52 a.m. same as appeared in the frequency deviation of Songkla.

As shown in Figure 13, the tie-line power flow from central area is kept between 250 MW and 350 MW from 3:00 a.m. to 6:30 a.m. This means that the HVDC link has been tripped for three and a half hours. At 6:30 a.m. the HVDC link is recovered and started to receive power from TNB again. At this moment, the tie-line power flow is still at 320.2 MW. Until 6:39 a.m. the power received by HVDC link reaches 300 MW. As seen in

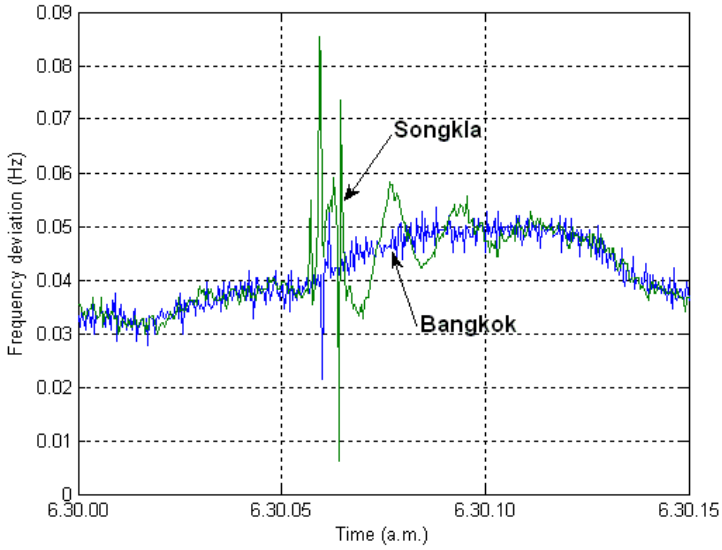

FIGURE 18. Frequency deviations of Bangkok and Songkla

Figure 13, the tie-line power flow from central area to southern area reduces from 320.2 MW at 6:30 a.m. to 25 MW at 7:00 a.m. Load demands in the southern area are mainly supplied by the imported power from TNB via HVDC link. In the same way, the phase difference between Bangkok and Songkla recorded by PMUs suddenly decreases due to the operation of HVDC link at 6:30 a.m. as shown in Figure 17. This explains that the power flow from central area also reduces. Subsequently, the phase difference between two sites tends to decrease while the tie-line power from central area also decreases. It should be noted that the variation of phase difference measured by PMUs changes in the same fashion as that of the actual tie-line power flow. Figure 18 depicts the frequency deviations of Bangkok and Songkla during the recovery of HVDC link. The inter-area mode also appears in the frequency deviation of Songkla. The frequency characteristic of frequency deviation analyzed by the short time Fourier transform is demonstrated in Figure 19. The dominant frequency of the inter-area mode at 0.5-0.6 Hz occurs at 6:30 a.m. same as in the frequency deviation.

The motivation of the practical use of the results obtained can be addressed as follows.

1) The real-time monitoring and control of the wide area power systems under the abnormal situations can be established based on the analyzed results. The early indication of grid problems such as abnormal angle difference, inter-area oscillation, voltage stability can be detected. Besides, they enable system operators to assess stress on the grid and take timely actions.

2) The post-disturbance analysis can be carried out based on the study results. As a consequence, quick troubleshooting of power-outage events can be performed.

3) Benchmarking, system model, validation and fine-tuning. Better model parameters based on PMU data allow for more accurate computation of control actions, identity errors in system modeling data and for fine-tuning power system models for both online and offline applications such as power flow, stability, short circuit, optimal power flow, security assessment, modal frequency response.

4) Power system restoration. Based on analyzed results, timely and proper decision to bring equipment back into service without risking stability or unsuccessful reclosing attempts can be carried out. Besides, the ability to directly measure system conditions,

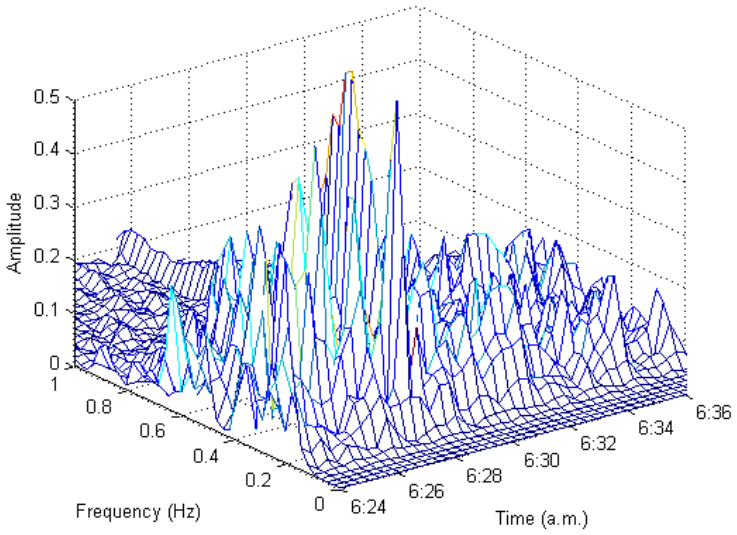

FIGURE 19. Frequency characteristic of frequency deviation analyzed by short time Fourier transform

e.g., operator knows if it is feasible to reclose the tie-line or reconnect substation is obtained. This is valuable tool which increases confidence level for operator who is under pressure to reenergize the grid.

5) Real-time automated control. The analyzed results are beneficial for automated prevention of angular stability, voltage stability, low-frequency oscillations and thermal constraints can be achieved. Additionally, the analyzed results also support optimized and integrated control with power electronics devices.

7. **Identification of Power Oscillation Mode.** To identify the dominant power oscillation mode from the phase difference data, the reduced 2^{nd} order model is applied. Consider the power swing equations of generators in an n-machine power system [41].

$$M_i\dot{\omega}_i = -D_i\left(\omega_i - 1\right) + P_{mi} - P_{ei} \tag{12}$$

$$\dot{\delta}_i = \omega_r\left(\omega_i - 1\right) \tag{13}$$

where $i = 1, 2, \ldots, n$, ω is a per unit angular velocity, δ is a rotor angle, M is an inertia constant, D is a damping coefficient, P_m is a mechanical input to the generator, P_e is an electrical output, and $\omega_r = 2\pi f$ is a base angular velocity. The dynamic characteristics of the reduced system embedded with the dominant inter-area mode can be represented by the 2^{nd} order swing equation in terms of the phase angle difference as

$$\dot{x}_1 = \frac{\omega_r}{M}\left(-D\left(\omega - 1\right) + P_m - P_e\right) \tag{14}$$

$$\dot{x}_2 = x_1 \tag{15}$$

where $x_1 = \dot{\delta} - \dot{\delta}_0$, $x_2 = \delta - \delta_0 - (\delta_{ini} - \delta_{0,ini})$, δ and δ_0 are phase angles at PSU and KMITL, respectively, $\dot{\delta}$ and $\dot{\delta}_0$ are the first derivatives of phase angles at PSU and KMITL, respectively, the subscript "*int*" is the initial value of phase angle.

When the power system works under the equilibrium condition, the primary disturbance comes from the load change. The load changes are usually distributed, random, and of small amplitude. As the amplitude of the disturbance is small, the nonlinear power system can be approximated by a linear model around a given operating point. Based on this assumption, the linearized model of the system based on ambient data can be applied

to obtain point estimates of electromechanical modes of power system working under equilibrium condition.

Accordingly, a small change in electrical power deviation due to phase angle difference can be represented by

$$\Delta P_e = -K\left(\delta - \delta_0\right) \tag{16}$$

where K is a synchronizing power coefficient. Assume that a mechanical power input is constant. A mechanical power deviation ΔP_m becomes zero. Linearizing (14) and (15) and expressing in terms of $\delta - \delta_0$ yields

$$\ddot{\delta} - \ddot{\delta}_0 = -\frac{D}{M}\left(\dot{\delta} - \dot{\delta}_0\right) - \frac{K}{M}\left(\delta - \delta_0\right) \tag{17}$$

where $\ddot{\delta}$ and $\ddot{\delta}_0$ are the second derivatives of phase angles at PSU and KMITL, respectively. By applying the wavelet decomposition based on Symlet wavelet functions with 12 levels to the measured data $\ddot{\delta} - \ddot{\delta}_0$, $\dot{\delta} - \dot{\delta}_0$ and $\delta - \delta_0$, extracting the d5 element of each term and substituting in (17), the coefficients D/M and K/M can be estimated by a least-squares regression.

Because (17) is the 2nd order differential equation, the characteristic equation can be represented by

$$s^2 + 2\zeta\omega_n s + \omega_n^2 = 0 \tag{18}$$

Hence, the undamped natural frequency (ω_n) and the damping ratio (ζ) are determined by

$$\omega_n = \sqrt{\frac{K}{M}} \tag{19}$$

$$\zeta = \frac{D}{2M\omega_n} \tag{20}$$

The undamped natural frequency and the damping ratio lead to the calculation of the eigenvalues. Suppose that the eigenvalues corresponding to the oscillation mode are $-\sigma \pm j\omega_d$, the real part (σ) and the imaginary part (ω_d) of the eigenvalues can be determined by

$$\sigma = \zeta\omega_n \tag{21}$$

$$\omega_d = \omega_n\sqrt{1 - \zeta^2} \tag{22}$$

To validate that the dynamic characteristics of the dominant inter-area mode of the actual power system can be conserved in the reduced 2nd order model, the least-square regression is applied. Consider the six-machine longitudinal interconnected power system as shown in Figure 20. Each generator is equipped with an exciter as depicted in Figure 21. Governor is neglected in this model. For the load characteristic, it is represented by the constant current characteristic model. The generator rated capacities are set as in Table 5, so that the inter-area oscillation mode between both end generators tends to be dominant. Eigenvalue analysis of this system is carried out by EUROSTAG [42].

Next, to construct the reduced 2nd order model (17), the time series data of the phase angle difference $\delta - \delta_0$, which can be obtained by time domain simulation, is used. By varying system loads slowly, the small oscillation of the phase angle difference can be provoked. Here, phase difference data of 200 second simulation time are used for estimating the eigenvalues. Consequently, the original eigenvalues calculated from EUROSTAG and the eigenvalues estimated by the reduced 2nd order system corresponding to the dominant inter-area mode of three case studies are shown in Table 6. The original eigenvalues are almost equal to the estimated eigenvalues for all cases. This confirms the validity of the reduced 2nd order model for estimating the dominant eigenvalues.

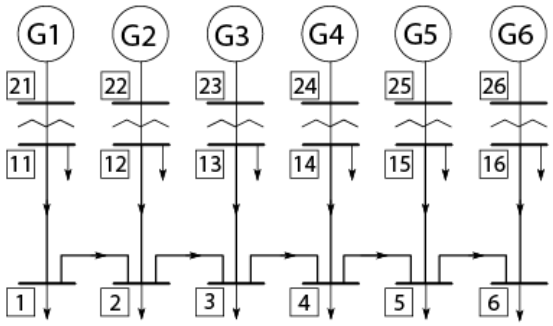

FIGURE 20. Six-machine longitudinal multi-machine system

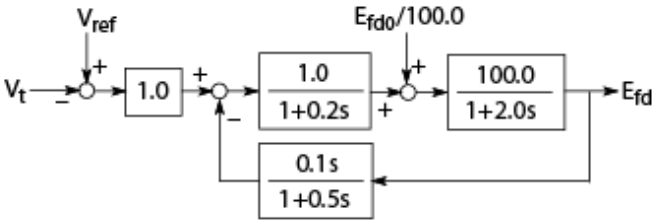

FIGURE 21. Exciter model

TABLE 5. Generator power capacity

Generator	Case 1 (MVA)	Case 2 (MVA)	Case 3 (MVA)
G1	20,000	16,000	12,000
G2	13,500	10,800	8,000
G3, G5	6,750	5,400	4,000
G4	40,000	32,000	24,000
G6	33,000	27,000	20,000
Total sum	120,000	96,600	72,000

TABLE 6. Eigenvalue analysis results

	Case 1	Case 2	Case 3
Original (EUROSTAG)	$-0.09 \pm j1.93$	$-0.13 \pm j2.85$	$-0.16 \pm j3.21$
Estimate (2^{nd} Order Model)	$-0.09 \pm j1.94$	$-0.13 \pm j2.84$	$-0.16 \pm j3.18$

As an example, the phase difference from 8.20 p.m. to 8.40 p.m. on June 4, 2005 is employed to identify the reduced 2^{nd} order system. As a result, the estimated values of D/M and K/M are equal to 0.3617 and 8.9480, respectively. To evaluate the regression results, the d5 elements of $\ddot{\delta} - \ddot{\delta}_0$ is substituted in the left side of (17), while the estimated D/M, K/M and the d5 elements of $\dot{\delta} - \dot{\delta}_0$ and $\delta - \delta_0$ are substituted in the right side of (17). Figure 22 shows the comparison results of the measured values (the left side of (17)) and the estimated values (the right side of (17)). Clearly, the measured values are almost equal to the estimated values. Consequently, the eigenvalues corresponding to the

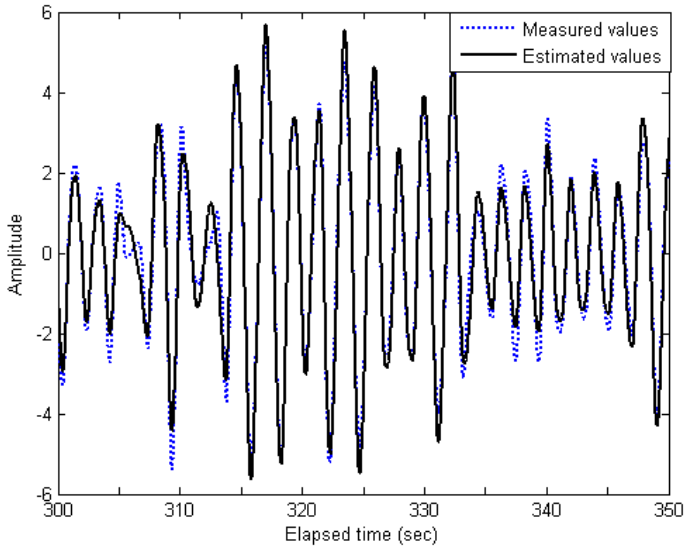

FIGURE 22. Comparison of measured values and estimated values

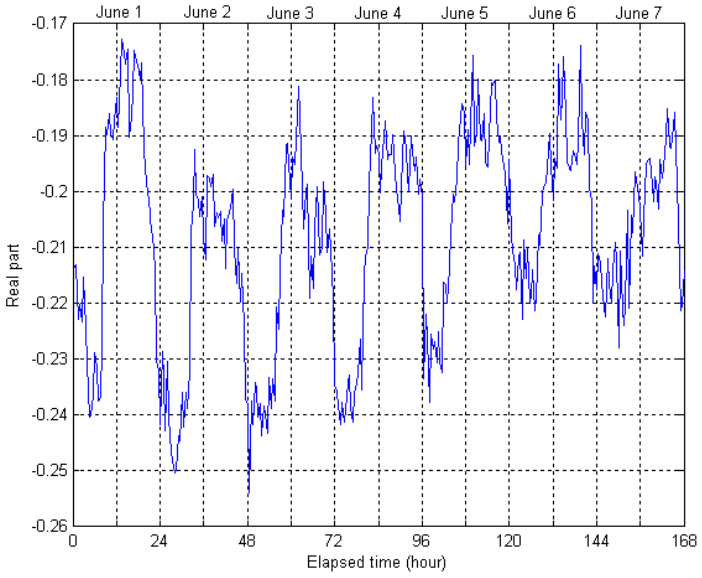

FIGURE 23. Variation of real part of eigenvalue, June 1 – 7, 2005

oscillation mode from 8.20 p.m. to 8.40 p.m. on June 4, 2005 are $-0.1808 \pm j2.9858$. The oscillation frequency is 2.9858 rad/sec (0.4752 Hz) and the damping ratio is 0.0605.

Next, the behavior of the inter-area mode is monitored by the variations of eigenvalues in each considered period. Figures 23 and 24 illustrate the variations of real part and imaginary part of eigenvalues from June 1 to 7, 2005, respectively. The real part of eigenvalues is negative throughout this period. This implies the positive damping of eigenvalues and stable system. Besides, the variation of the real part on each day has almost the same pattern. In the nighttime, the oscillation mode is more stable than that in the daytime. This is due to large power demands in the daytime which deteriorate the system stability. For the imaginary part which is the oscillation frequency, it also varies in the same way on each day. The oscillation frequency in the daytime is lower than that in

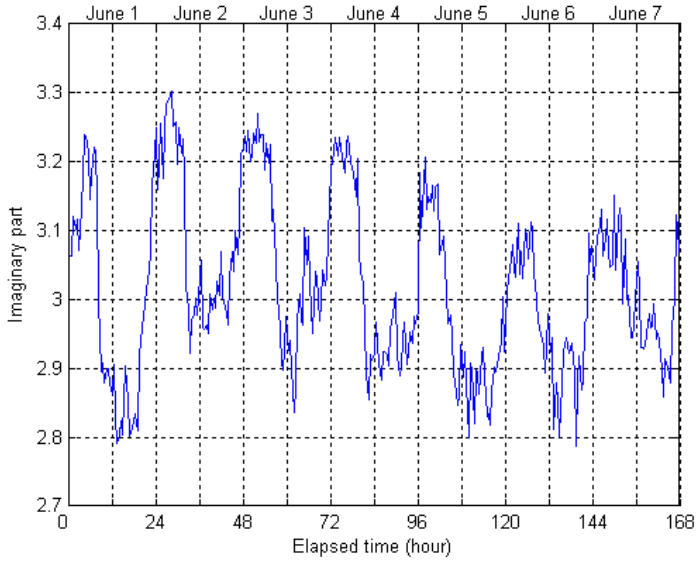

FIGURE 24. Variation of imaginary part of eigenvalue, June 1 – 7, 2005

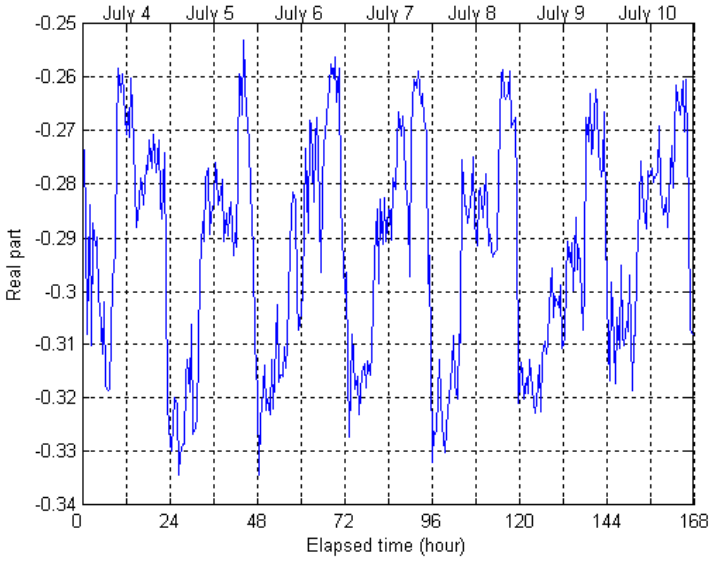

FIGURE 25. Variation of real part of eigenvalue, July 4 – 10, 2005

the nighttime. This is because the participation of synchronous generators in the daytime is higher. This is equivalent to a larger system inertia which leads to a longer oscillation period and a lower oscillation frequency (see (19) and (20)). On the other hand, the oscillation frequency in the nighttime becomes larger due to low power demands. Figures 25 and 26 depict the variations of real part and imaginary part of eigenvalues from July 4 to 10, 2005, respectively. The oscillatory behavior can be described as in the former period. These results exhibit that the wide area stability based on monitoring of power oscillation mode can be accessed from the phasor measurement taken at typical power outlets.

8. **Conclusion.** In this paper, an application of discrete wavelet decomposition and short-term Fourier transform to analyze power system dynamic events based on the 220 V

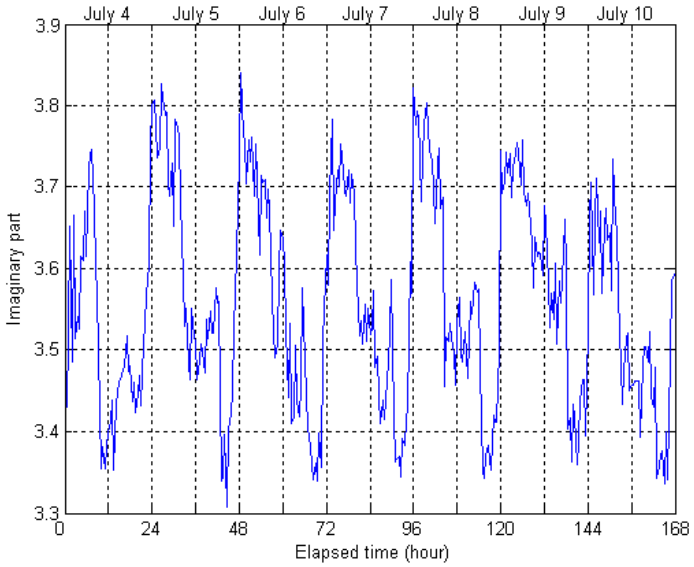

FIGURE 26. Variation of imaginary part of eigenvalue, July 4 – 10, 2005

wall outlet based-monitoring system using synchronized PMUs has been presented. Two dynamic events of Thailand and Malaysia power systems, i.e., the load transferring with system synchronization and the tripping event of HVDC link has been analyzed by the PMU data. The validity of the measured phase difference by synchronized PMU is verified by comparing to the active power flow of EGAT. The discrete wavelet decomposition and the short-time Fourier Transform have been applied to analyze the frequency deviation characteristic in both time and frequency domains. It is found that the dominant frequency of the dominant inter-area mode is around 0.4-0.6 Hz. In addition, the dynamic events also cause the inter-area oscillation mode in a 230 kV tie-line to severely oscillate. Analyzed results from this study are very useful for practical operation of Thailand and Malaysia systems.

Acknowledgement. This work was supported by the King Mongkut's Institute of Technology Ladkrabang Research Fund.

REFERENCES

[1] G. Roger, *Power System Oscillations*, Springer, 1999.
[2] M. M. Al-Harthi, Robust AVR design based on mixed H_2/H_∞ pole placement using linear matrix inequality (LMI), *ICIC Express Letters*, vol.4, no.3(B), pp.963-971, 2010.
[3] L.-Y. Sun, J. Zhao and G. M. Dimirovski, Nonlinear robust controller design for thyristor controlled series compensation, *International Journal of Innovative Computing, Information and Control*, vol.5, no.4, pp.981-989, 2009.
[4] A. G. Phadke, Synchronized phasor measurements in power systems, *IEEE Computer Application in Power*, vol.6, no.2, pp.10-15, 1993.
[5] K. E. Martin et al., IEEE standard for synchrophasors for power systems, *IEEE Transactions on Power Delivery*, vol.13, no.1, pp.73-77, 1998.
[6] J. F. Hauer, D. Trudnowski, G. Rogers, W. A. Mittelstadt, W. H. Litzenberger and J. Johnson, Keeping an eye on power system dynamics, *IEEE Computer Application on Power*, vol.10, no.4, pp.50-54, 1997.
[7] J. F. Hauer, N. B. Bhatt, K. Shah and S. Kolluri, Performance of WAMS East in providing dynamic information for the North East blackout of August 14, 2003, *Proc. of 2004 IEEE PES General Meeting*, vol.2, pp.1685-1690, 2004.

[8] C. Rehtanz, Tack force on Wide area monitoring and control for transmission capability enhancement, *CIGRE WG C4.6.01*, 2006.
[9] R. O. Burnett, M. M. Butts, T. W. Cease, V. Centeno, G. Michel, R. J. Murphy and A. G. Phadke, Synchronized phasor measurements of a power system event, *IEEE Transactions on Power Systems*, vol.9, no.3, pp.1643-1650, 1994.
[10] C. W. Liu, J. S. Thorp, J. Lu, R. J. Thomas and H. D. Chiang, Detection of transiently chaotic swings in power systems using real-time phasor measurements, *IEEE Transactions on Power Systems*, vol.9, no.3, pp.1285-1292, 1994.
[11] Z. Zhong, C. Xu, B. J. Billian, L. Zhang, S.-J. S. Tsai, R. W. Conners, V. A. Centeno, A. G. Phadke and Y. Liu, Power system frequency monitoring network (FNET) implementation, *IEEE Transactions on Power Systems*, vol.20, no.4, pp.1914-1921, 2004.
[12] R. Tsukui, P. Beaumont, T. Tanaka and K. Sekiguchi, Power system protection and control utilizing Intranet technology, *Power Engineering Journal*, vol.15, pp.249-255, 2001.
[13] TOSHIBA Corporation, *PMU Document*, 2001.
[14] X. Xie, Y. Xin, J. Xiao, J. Wu and Y. Han, WAMS applications in Chinese power systems, *IEEE Power & Energy Magazine*, vol.4, no.1, pp.54-63, 2006.
[15] J. Rasmussen and P. Jorgensen, Synchronized phasor measurements of a power system event in Eastern Denmark, *IEEE Transactions on Power Systems*, vol.21, no.1, pp.278-283, 2006.
[16] J. Y. Cai, Z. Huang, J. Hauer and K. Martin, Current status and experience of WAMS implementation in North America, *Proc. of 2005 Asia and Pacific IEEE/PES Transmission & Distribution Conference Exhibition*, pp.1-7, 2005.
[17] H. Lee, C. Lim, S. Lee, K. Kim, T. Kim, J. Shin and S. Nam, Development of an intelligent voltage control system for Korean power systems, *ICIC Express Letters*, vol.3, no.4(B), pp.1315-1320, 2009.
[18] Y. Zhang, Z. Wang and J. Zhang, Electric power system fault detection based on posterior probability, *ICIC Express Letters*, vol.6, no.7, pp.1721-1725, 2012.
[19] Y. Zhang, Z. Wang and J. Zhang, A statistical evaluation of power grid fault detection, *ICIC Express Letters, Part B: Applications*, vol.3, no.1, pp.47-52, 2012.
[20] Y. Zhang, L. Zhang, J. Zhang and Z. Wang, Fault detection based on correlation analysis theory in complex power systems, *ICIC Express Letters, Part B: Applications*, vol.2, no.3, pp.751-756, 2011.
[21] C. S. Burrus, R. A. Gopinath and H. Guo, *Introduction to Wavelets and Wavelet Transforms: A Primer*, Prentice Hall, 1997.
[22] Z. Zhang, J. Ohtaki, H. Toda, T. Imamura, T. Miyake and Y. Ishikawa, A study of abnormal signal extraction by using parasitic discrete wavelet transform, *ICIC Express Letters*, vol.6, no.4, pp.999-1004, 2012.
[23] C.-Y. Song, Y.-L. Qiao and X.-Z. Zhang, Image encryption algorithm based on chaos and integer wavelet transform, *ICIC Express Letters*, vol.6, no.2, pp.403-409, 2012.
[24] C.-Y. Yang, Robust reversible data hiding scheme based on integer wavelet transform, *ICIC Express Letters*, vol.5, no.11, pp.4209-4214, 2011.
[25] D. Li, M. Diao and L. Wei, The design and analysis of network traffic methods based on multifractal wavelet modeling, *ICIC Express Letters*, vol.5, no.8(A), pp.2699-2704, 2011.
[26] C. Pothisarn, C. Jettanasen, A. Ngaopitakkul and C. Apisit, Identification of fault location for simultaneous fault in distribution system using discrete wavelet transform, *ICIC Express Letters*, vol.5, no.4(B), pp.1423-1428, 2011.
[27] S. Liu, J. Pu, H. Zhang and L. Zhao, Wavelet-based hemodynamic analyzing method for FMRI data, *ICIC Express Letters*, vol.5, no.3, pp.595-600, 2011.
[28] C. Hu and P. Zhang, Improved wavelet-based contourlet transform and its application to image fusion, *ICIC Express Letters*, vol.5, no.3, pp.823-828, 2011.
[29] X. Luo, F. Liu, X. He and C. Yang, Classification of Stego and PS images based on wavelet decomposition and filtering, *ICIC Express Letters*, vol.4, no.3(B), pp.1005-1010, 2010.
[30] H. Guo, J.-Y. Zhao, N. Jiang and L. Shi, Chinese minority script identification using wavelets transform and SVM, *ICIC Express Letters*, vol.4, no.3(A), pp.653-658, 2010.
[31] Z. Li and Y. Wang, Classification of sound types in border monitoring system based on wavelet transform, *ICIC Express Letters, Part B: Applications*, vol.3, no.1, pp.127-132, 2012.
[32] J. Dong, X. Wei, Q. Zhang and Y. Zhao, Pitch detection using circular average magnitude difference function based on wavelet transform, *International Journal of Innovative Computing, Information and Control*, vol.5, no.9, pp.2717-2724, 2009.
[33] R. Bracewell, *The Fourier Transform & Its Applications*, 3rd Edition, McGraw-Hill, 1999.

[34] N. Yoshikawa and S. Yamazaki, Fourier-transform-based three-dimensional profile acquisition method implemented by graphics processing unit, *ICIC Express Letters*, vol.4, no.3(A), pp.697-703, 2010.
[35] X. Meng, L. Li, S. Li and E. Ding, Vibration signal recognition based on Fourier analysis for underground environments, *ICIC Express Letters, Part B: Applications*, vol.3, no.2, pp.367-373, 2012.
[36] The MathWorks, *MATLAB Wavelet Toolbox*, User's Guide, 2005.
[37] The MathWorks, *MATLAB Signal Processing Toolbox*, User's Guide, 2005.
[38] The MathWorks, *MATLAB Statistic Toolbox*, User's Guide, 2005.
[39] R. Zhang, H. Han, Y. Zhang and X. Liang, Degree reduction of B-spline curves with multiple knots using least squares approximation, *ICIC Express Letters*, vol.5, no.9(A), pp.3243-3248, 2011.
[40] *http://www.egat.co.th/hvdc/*.
[41] P. Kundur, *Power System Stability and Control*, McGraw Hill, 1994.
[42] *EUROSTAG Release 4.1 Package Documentation, Parts I and II, Tractebel-EDF*, 2000.